



ELSEVIER

Available online at [www.sciencedirect.com](http://www.sciencedirect.com)

SCIENCE @ DIRECT®

Earth and Planetary Science Letters 228 (2004) 143–160

EPSL

[www.elsevier.com/locate/epsl](http://www.elsevier.com/locate/epsl)

# The Central Atlantic Magmatic Province at the Triassic–Jurassic boundary: paleomagnetic and $^{40}\text{Ar}/^{39}\text{Ar}$ evidence from Morocco for brief, episodic volcanism

K.B. Knight<sup>a,\*</sup>, S. Nomade<sup>a,b</sup>, P.R. Renne<sup>a,b</sup>, A. Marzoli<sup>c</sup>, H. Bertrand<sup>d</sup>, N. Youbi<sup>e</sup>

<sup>a</sup>Department of Earth and Planetary Science, University of California, Berkeley, CA 94720, USA

<sup>b</sup>Berkeley Geochronology Center, 2455 Ridge Rd., Berkeley, CA 94709, USA

<sup>c</sup>Dipartimento di Mineralogia e Petrologia, Università di Padova, I-35137 Italy

<sup>d</sup>Laboratoire des Sciences de la Terre, Ecole Normale Supérieure de Lyon et UCBL, Lyon, France

<sup>e</sup>Department of Geology, Faculty of Sciences-Semlalia, Cadi Ayyad University, Marrakech, Morocco

Received 29 March 2004; received in revised form 27 July 2004; accepted 4 September 2004

Available online 27 October 2004

Editor: V. Courtillot

## Abstract

The Central Atlantic Magmatic Province (CAMP), one of the largest known flood basalt provinces formed in the Phanerozoic, is associated with the pre-rift stage of the Atlantic Ocean at the Triassic–Jurassic boundary ca. 200 Ma. Paleomagnetic sampling targeted packages of CAMP lava flows in Morocco's High Atlas divided into four basic units (the lower, intermediate, upper, and recurrent units) from sections identified on the basis of field observations and geochemistry. Oriented cores were demagnetized using both alternating field (AF) and thermal techniques. Paleomagnetic results reveal wholly normal polarity interrupted by at least one brief reversed chron located in the intermediate unit, and reveal distinct pulses of volcanic activity identified by discrete changes in declination and inclination. These variations in magnetic direction are interpreted as a record of secular variation, and they may provide an additional correlative tool for identification of spatially separated CAMP lava flows within Morocco.  $^{40}\text{Ar}/^{39}\text{Ar}$  analyses of Moroccan CAMP lavas yield plateau ages indistinguishable within  $2\sigma$  error limits, sharing a weighted mean age of  $199.9 \pm 0.5$  Ma ( $2\sigma$ ), reinforcing the short-lived nature of these eruptions despite the presence of sedimentary horizons between them. Correlation of our sections with the E23n, E23r, E24 sequence reported in the Newark basin terrestrial section and St. Audrie's Bay marine section is suggested. Brief volcanism in sudden pulses is a potential mechanism for volcanic-induced climatic changes and biotic disruption at the Triassic–Jurassic boundary. Combination of our directional group (DG) poles yields an African paleomagnetic pole at 200 Ma of  $\lambda(^{\circ}\text{N})=73.0^{\circ}$ ,  $\phi(^{\circ}\text{E})=241.3^{\circ}$  ( $Dp=5.0^{\circ}$ ,  $Dm=18.5^{\circ}$ ).

© 2004 Elsevier B.V. All rights reserved.

**Keywords:** Triassic–Jurassic; Central Atlantic Magmatic Province; paleomagnetism; geochronology; large igneous province

\* Corresponding author. Tel.: +1 510 643 4466; fax: +1 510 643 9980.

E-mail address: [kbk@uclink.berkeley.edu](mailto:kbk@uclink.berkeley.edu) (K.B. Knight).

## 1. Introduction

The Central Atlantic Magmatic Province or ‘CAMP’ [1] is primarily represented by dikes and sills in northeastern South America, northwestern Africa, southwestern Europe, and eastern North America (Fig. 1a) with an aerial extent of  $\sim 1 \times 10^7$  km<sup>2</sup>. Some of the most important lava flow outcrops, with total thicknesses of 100 to 300 m, are found in the Late Triassic to Early Jurassic basins located around northeastern North America and northeastern Africa (central Pangea). Estimates of the preerosional volume of CAMP lavas exceed  $2.5 \times 10^6$  km<sup>3</sup> [4],

easily comparable with large igneous provinces such as the Siberian Traps or Deccan Traps. Published <sup>40</sup>Ar/<sup>39</sup>Ar plateau ages (see online appendix) center on a main eruption at  $\sim 200$  Ma, and cyclostratigraphic studies in the North American Newark Supergroup indicate a brief eruptive duration ( $\sim 600$  kyr) for the main volcanic period [5]. Published paleomagnetic data from throughout CAMP are consistent with a brief magmatic event, as shown by the normal polarity of the vast majority of intrusive and extrusive CAMP rocks.

CAMP lavas in Morocco are found at the top of the Triassic sequence filling large Triassic–Jurassic

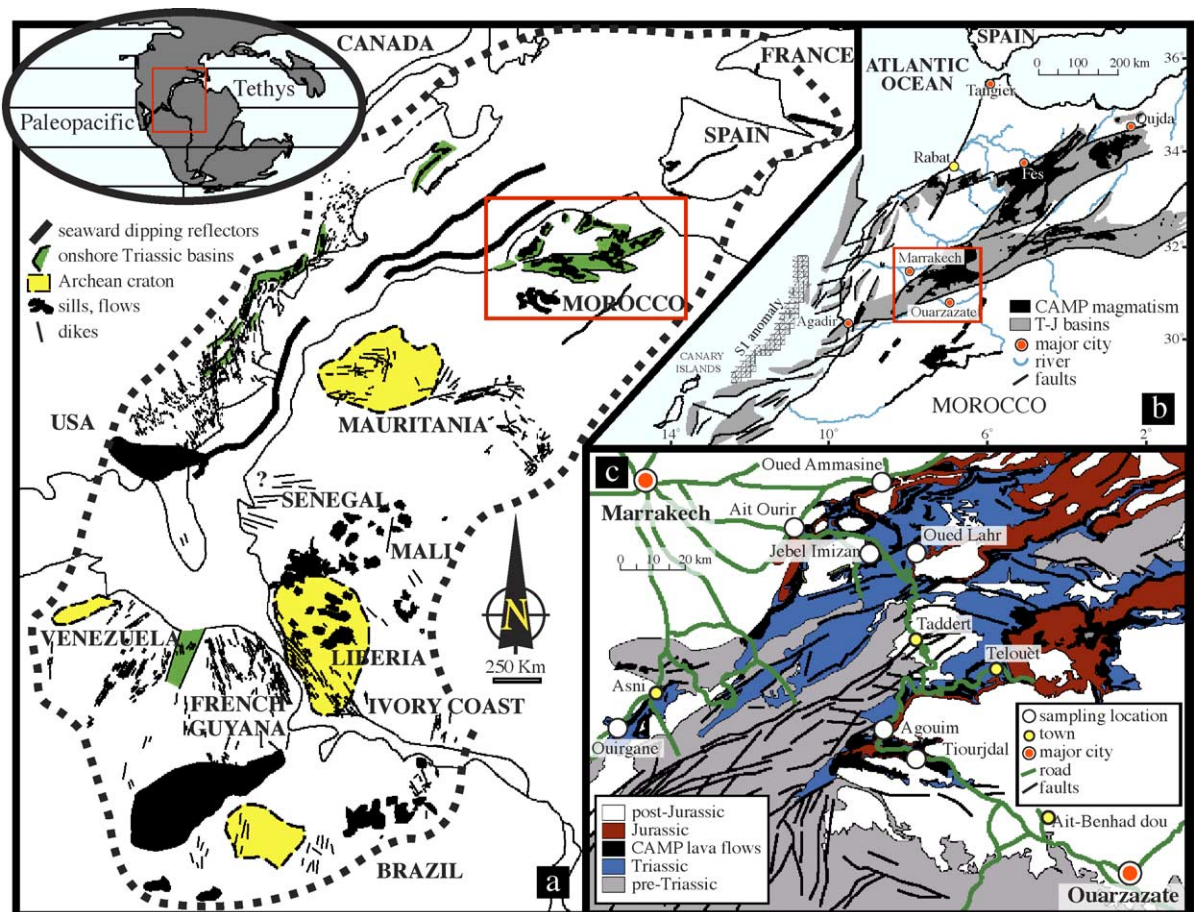


Fig. 1. (a) Preserved extent of the Central Atlantic Magmatic Province across four continents. Heavy dashed line shows the probable original extent affected. Mapping of intrusive activity is preliminary and some portions such as EW dikes of Senegal [2] are inferred from remote survey only. Inset shows an Early Jurassic continental reconstruction after [3], before initiation of mid-Atlantic rifting. (b) Triassic–Jurassic geology of Morocco, with rift zones, basin structures, and CAMP-related magmatism. (c) Sampling locations discussed in this paper, as well as the generalized High Atlas geology.

synrift basins (Fig. 1b) formed during lithospheric extension prior to the opening of the central Atlantic (e.g., [6,7]). CAMP lava flows are compositionally classified as low-Ti tholeiitic basalts and basaltic andesites [8,9], with formations displaying a time-dependent compositional trend towards incompatible element depleted compositions [9,10]. CAMP lava stratigraphy and correlation in Morocco [8] is based on field observations including the presence of sediments between flows and distinctive changes in flow texture, as well as published geochemical data [9,10]. From the base to the top, CAMP lava flows are divided into four primary units called the lower, intermediate, upper, and recurrent units [8], decreasing in total volume from the base to the top. The sedimentary layers occasionally found within or in between the lower, intermediate and upper units never exceed ~2 m thickness. The recurrent unit, where present, is made up of a massive, single flow separated from the upper unit flows by intraflow sediments up to 50 m in thickness.

The relation between the CAMP magmatic event and extinctions at the Triassic–Jurassic boundary has come increasingly into focus (e.g., [11–15]). Although recent review of the Triassic–Jurassic boundary questions the reliability of palynomorphs in defining the boundary (e.g., [16]), it has been proposed that volcanism commenced in the Newark Basin following the last appearance of typical Triassic pollens (e.g., *Patinasporites densus*) [17,18]. Recent studies suggest synchrony between the occurrence of CAMP volcanism and the major extinction event at the Triassic–Jurassic boundary [10,12].

This paper presents new paleomagnetic data and  $^{40}\text{Ar}/^{39}\text{Ar}$  ages from lava flows of the High Atlas Moroccan Triassic–Jurassic basins where CAMP volcanism is well represented, interstratified with synrift continental sediments and preserved from erosion. Six sections in the High Atlas mountains between the cities of Marrakech and Ouarzazate (Fig. 1b), referred to as the Tiourjidal, Ait Ourir, Jebel Imizar, Oued Lahr, Oued Ammasine and Agouim (Fig. 1c) were chosen to represent the most complete and continuous records of Moroccan CAMP volcanism available with visible flow contacts and minimal alteration. Sections are described in further detail sections online (see online appendix) and abbreviated paleomagnetic results from the

Tiourjidal section have been described previously [10]. The paleomagnetic and  $^{40}\text{Ar}/^{39}\text{Ar}$  data clarify the timing and eruptive style of the CAMP volcanism in Morocco, and are relevant to data from terrestrial lavas of similar age located in the northeastern United States basins [14], and with data from marine Triassic–Jurassic sections [19].

## 2. Analytical procedures

Depending on flow thickness, between 2 and 10 cores were drilled in each identified flow. Flow attitude was measured wherever possible to provide a basis for tilt correction. Flows varied from near horizontal (~10° dip) to having significant dip (~40° dip), making such measurements vital. A total of 425 cores yielding 560 analyzed specimens were included in this study. Core azimuths were measured by magnetic and solar compasses. The difference between these two measurements was used to calculate local declination (−1° to −8°, averaging −4°, in agreement with the calculated International Geomagnetic Reference Field declination) for recovered cores. Recovered cores were cut into lengths of 2–2.5 cm and were stored in a magnetically shielded room with an ambient field of less than ~200 nT for the remainder of the study.

Low-coercivity overprints were removed from all specimens by an applied field from 0 to 8 mT. At sections other than Tiourjidal, thermal demagnetization was performed on specimens from every core, and, where possible (~30% of all cores), alternating field (AF) demagnetization was also applied to a specimen from the same core. Thermal (247 specimens) and AF (148 specimens) demagnetization techniques were applied in 12 to 20 steps over peak fields of 10–130 mT or peak temperatures of 150 to 600 °C. Bulk susceptibility was measured after every, or every other heating step, to monitor mineral transformations during demagnetization. At Tiourjidal, hybrid demagnetization (using AF demagnetization up to 8 mT peak fields followed by heating to 150 °C for 1 h, and then continued progressive AF demagnetization steps) was applied to all 162 specimens to remove a possible component carried by high-coercivity minerals such as goethite. AF demagnetizations were performed using

a two-axis static demagnetizer online with a cryogenic magnetometer. Thermal demagnetization used a noninductively wound electrical resistance furnace. All measurements were made in the Berkeley Geochronology Center (BGC) paleomagnetic laboratory. Representative petrographic descriptions are available online.

A total of 11 flows from five sections (Fig. 1c) were selected for  $^{40}\text{Ar}/^{39}\text{Ar}$  geochronology. In order to date the same samples as those used for paleomagnetic analysis, we selected and crushed between three and five core samples sampled from the same flow that were either analyzed previously by AF demagnetization only, or were unanalyzed core remnants. After crushing, samples were sieved into two size fractions (125–180 and 180–260  $\mu\text{m}$ ) and washed ultrasonically in distilled water. Matrix, olivine, and pyroxene phenocrysts and plagioclase with inclusions were removed with a Frantz Isodynamic Separator, and ~20–30 mg of transparent plagioclase from each sample was handpicked under a binocular microscope. Samples were loaded into aluminum disks and irradiated for 5 h in the CLICIT facility of the TRIGA reactor at Oregon State University. Two separate irradiations were performed, each using two disks, referred to as ‘G’ and ‘H’ from the first irradiation, and ‘A’ and ‘B’ from the second irradiation (Background Data Set). After irradiation, ~10-mg samples of plagioclase were degassed in 8–24 steps using a defocused  $\text{CO}_2$  laser (Synrad) and integrator lens, and were analyzed with a MAP 215C mass spectrometer at the BGC.

Neutron fluence ( $J$ ) was monitored by coirradiation of the Fish Canyon sanidine standard placed in six positions around each aluminum sample irradiation disk. The  $J$  value was determined from individual analysis of 6 to 10 single grains of Fish Canyon sanidine from each disk position fused with a  $\text{CO}_2$  laser. The corresponding  $J$  values (see online appendix) calculated using the age of 28.02 Ma [20] and the total decay constants of [21], varied  $\leq 0.4\%$

across each of the four disks. Procedural backgrounds were measured every three degassing steps. Average blanks and signals for unknowns are given in the online appendix. Mass discrimination was monitored by automated analysis of over 150 air pipettes. Nucleogenic production ratios used to correct for reactor produced Ar isotopes from K and Ca were as in [22]. Plateau ages are defined as comprising three or more contiguous steps corresponding to a least 70% of the total  $^{39}\text{Ar}$  released and showing no significant slope, with the individual step ages agreeing within  $2\sigma$  errors with the weighted mean age of the plateau segment. Full analytical data corrected for backgrounds, mass discrimination, and radioactive decay are available online.

### 3. Paleomagnetic results

A total of ~560 specimens were measured, representing 68 lava flows or sediment horizons from six sections, of which 510 yielded stable directions (Table 1). The natural remanent magnetization (NRM) intensity ranged from 0.001 to 0.1 A/m. Typical demagnetization behavior for each unit, tilt-corrected, are plotted in stereographic projection (Fig. 2), along with relative magnetic intensity diagrams for thermal and AF demagnetization. Normal directions are also plotted as orthogonal vector endpoint (Zijderveld) diagrams [24], and are defined by least-squares line fits [25]. Reversed directions were defined using great circle fits [26]. Examples of thermal and AF demagnetization pairs on specimens from the same core are shown for each lava unit and yielded consistent directions throughout the study. Data were rejected for suspect directions (intraflow deviations  $>20^\circ$ ) if field or laboratory notes noted potential problems such as loose blocks, misorientation, or analytical difficulties. Mean flow directions were calculated

---

#### Notes to Table 1:

Mean flow directions were calculated using PaleoMac [23]. Direction groups for sections other than Tiourjidal are suggestions, determined by comparison with the Tiourjidal section.  $n$ : total number of analyses in the flow used to calculate the mean direction;  $N$ : total number of analysis in the flow;  $D_{\text{geo}}$ ,  $I_{\text{geo}}$ : declination and inclination in geographic coordinates;  $D_{\text{str}}$ ,  $I_{\text{str}}$ : declination and inclination with applied bedding-tilt correction;  $k$ : precision parameter;  $A_{95}$ : 95% confidence limit on the mean direction;  $\text{VGP}_{\text{lat}}$ ,  $\text{VGP}_{\text{long}}$ : virtual geomagnetic pole latitude and longitude; polarity: N=normal, R=reversed; DG: directional group associations, entries in italics are hypothetical and inferred from correlation to the Tiourjidal section; entries in gray type are not considered to yield reliable directions, see text for further detail.

Table 1  
Mean flow directions for all sections

unit	flow	n	N	D <sub>geo</sub> (°)	I <sub>geo</sub> (°)	D <sub>str</sub> (°)	I <sub>str</sub> (°)	k	A <sub>95</sub> (°)	VGP <sub>Long</sub> (°)	VGP <sub>Lat</sub> (°)	polarity	DG
Tiourjidal (N31 07' 43", W007 22' 43")													
low	1	6	6	358.6	20.0	355.6	33.9	239	4.3	205.9	76.8	N	1
low	2	3	3	1.5	19.8	358.9	33.9	422	5.0	192.3	77.5	N	1
low	3	4	4	358.9	20.3	355.9	34.2	457	4.3	205.2	77.1	N	1
low	4	4	4	3.1	19.0	0.8	33.3	418	4.5	183.8	77.1	N	1
low	5	3	3	3.5	19.1	1.2	33.4	759	4.5	182.3	77.1	N	1
low	6	4	5	358.3	23.2	354.8	36.9	640	3.6	212.4	78.5	N	1
low	7	5	5	358.1	23.4	354.6	37.2	251	4.8	213.9	78.6	N	1
low	8	6	7	0.3	23.9	357.0	37.9	218	4.5	203.3	79.8	N	1
low	9	6	6	9.4	30.0	7.0	44.7	172	5.0	133.3	82.2	N	2
low	10	4	5	13.7	30.7	12.2	45.6	380	4.7	115.0	78.6	N	2
low	11	4	5	8.0	29.6	5.8	44.2	286	4.5	141.3	82.7	N	2
low	12	4	4	10.6	29.5	8.6	44.3	213	6.3	129.3	81.0	N	2
low	13	4	5	8.6	31.8	5.9	46.4	842	2.6	129.0	83.8	N	2
low	14	4	4	8.7	29.9	6.2	44.6	1114	2.8	137.5	82.7	N	2
low	15	3	3	4.3	33.0	0.5	47.3	68	8.5	178.2	87.3	N	2
low	16	3	3	10.5	33.7	8.0	48.4	181	9.2	109.0	82.9	N	2
low	17	4	4	7.0	31.4	4.0	45.9	413	4.5	143.7	84.9	N	2
low	18	6	6	12.0	30.5	10.2	45.4	577	2.8	120.2	80.1	N	2
low	19	4	4	13.0	31.2	11.3	46.1	294	5.4	115.0	79.5	N	2
low	20	3	3	12.5	29.7	7.9	44.6	315	7.0	121.8	79.3	N	2
low	21	5	6	17.3	32.3	15.9	44.2	202	5.4	113.7	75.1	N	2
low	22	5	5	15.8	30.9	14.2	42.7	332	4.2	120.7	76.0	N	2
int	23	4	4	341.1	29.8	335.7	37.5	283	4.6	258.4	66.0	N	3
int	24	4	4	336.4	32.5	331.1	38.5	216	5.2	264.4	62.5	N	3
int	25	4	4	335.6	32.6	330.0	38.7	184	6.8	265.6	61.7	N	3
int	26	5	6	343.7	26.8	338.7	35.5	109	7.4	251.5	67.6	N	3
sed	27	3	4	130.7	-43.5	119.1	-45.6	*	4.1	109.4	-37.3	R	4
int	28	6	6	337.9	39.4	329.0	46.9	121	6.1	277.3	64.6	N	5
int	29	5	6	340.7	42.2	331.2	50.1	348	4.1	284.5	65.4	N	6
int	30	6	6	337.1	48.6	327.5	48.6	338	2.8	282.8	62.0	N	6
int	31	4	4	337.9	39.5	329.0	47.0	256	5.8	279.2	63.0	N	6
int	32	3	3	335.8	39.9	326.5	47.0	338	6.7	280.4	60.9	N	6
upp	33	7	7	341.7	41.0	332.8	49.1	66	6.4	281.7	66.6	N	6
upp	34	8	8	338.2	35.2	330.6	42.9	91	6.4	271.2	63.4	N	6
Agouim (N31 09' 47", W007 27' 59")													
sed	1	7	7	337.0	38.3	339.7	31.3	323	3.4	229.4	66.7	N	7
rec	2	20	20	334.1	39.3	337.1	32.4	230	2.2	234.7	65.2	N	7
Oued Ammassine (N31 40' 00", W007 20' 14")													
low	1	11	12	51.5	63.0	16.9	21.4	43	7.0	131.8	64.1	N	2
low	2	4	6	56.1	65.2	7.8	26.7	78	10.5	148.7	71.0	N	2
Ait Ourir (N31 32' 51", W007 40' 25")													
low	1	15	16	338.5	23.0	339.4	43.0	104	3.8	247.7	70.8	N	1
low	2	7	9	352.3	10.7	354.7	29.7	126	5.4	190.8	73.8	N	1
low	3	9	10	347.0	16.9	349.3	36.4	258	3.2	215.5	75.3	N	1
low	4	9	9	346.8	18.3	349.2	37.8	112	4.9	218.5	76.0	N	1
int	5	11	11	316.0	11.0	315.1	37.9	112	4.3	259.1	48.8	N	3
int	6	16	17	312.7	9.1	311.1	35.8	207	2.6	259.6	44.8	N	3
int	7	11	18	314.3	1.7	308.9	41.3	75	5.3	265.7	44.5	N	3
upp	8	12	14	313.3	19.3	307.4	50.8	173	3.3	276.7	45.7	N	6
rec	9	19	19	322.0	38.1	312.5	62.6	36	5.7	294.6	51.1	N	7
Jebel Imtizar (N31 36' 08", W007 26' 00")													
low	1	19	19	35.7	35.0	23.9	28.3	132	2.9	114.2	62.7	N	2
upp	2	17	17	343.3	71.8	329.7	42.8	473	1.6	255.7	62.5	N	6
upp	3	16	16	345.6	65.2	337.5	30.4	35	6.3	230.8	64.5	N	6
Oued Lahr (N31 36' 41", W007 22' 47")													
low	1	6	6	32.9	50.5	7.7	41.9	819	2.3	128.1	79.9	N	2
low	2	6	6	34.1	50.1	8.7	42.1	247	4.3	123.8	79.4	N	2
low	3	6	6	34.4	46.5	11.7	39.1	476	3.1	122.2	75.9	N	2
low	4	3	4	33.8	39.9	15.5	33.2	88	13.2	122.9	70.5	N	2
low	5	6	6	38.3	44.0	16.4	38.5	177	5.1	112.7	72.4	N	2
low	6	9	9	29.9	48.5	7.0	39.2	221	3.5	137.5	78.7	N	2
int	7	4	8	146.6	-71.3	146.6	-42.2	*	9.8	93.8	-61.8	R	4
int	8	7	8	348.1	54.7	340.2	36.5	612	2.4	234.8	69.0	N	5
int	9	5	7	351.8	43.6	346.4	25.7	51	10.8	210.2	68.0	N	5
int	10	7	9	355.2	47.4	351.6	27.9	156	4.8	199.1	71.6	N	5
int	11	8	10	348.3	46.7	346.4	26.9	134	4.8	211.4	68.6	N	5
int	12	19	21	351.4	43.2	348.4	33.8	81	3.7	205.5	69.0	N	5
int	13	18	20	355.6	54.4	317.5	48.0	154	2.9	269.7	53.4	N	6
upp	14	6	8	357.3	55.8	313.1	51.4	182	5.0	276.1	50.4	N	6
upp	15	6	6	345.2	48.9	316.3	39.5	125	6.0	260.3	50.3	N	6
upp	16	11	11	351.5	53.6	313.3	50.3	153	3.7	274.6	50.4	N	6
upp	17	7	9	339.5	61.4	306.4	51.1	50	8.6	277.6	45.0	N	6
upp	18	20	20	349.3	55.9	311.5	53.1	168	2.7	278.9	49.5	N	6

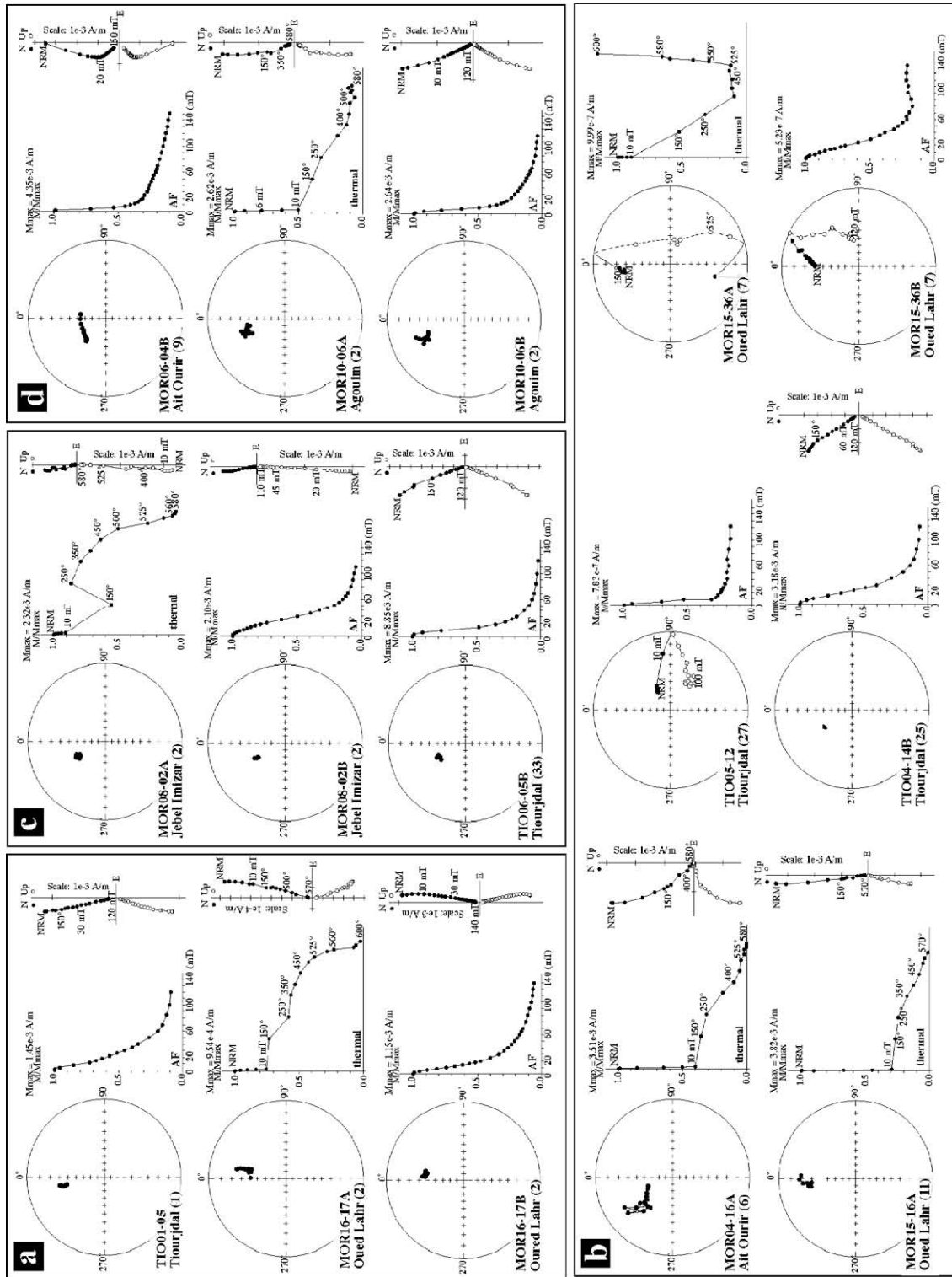


Fig. 2. Representative tilt-corrected results of thermal and alternating field demagnetization, plotted as orthogonal vector endpoint diagrams and in equal area projection: (a) lower, (b) intermediate, (c) upper, and (d) recurrent units.

using Fisher statistics [27]. Tilt corrections were applied, as measured on bedding structures in the field, to each flow.

Lower-unit specimens (218 specimens from 184 cores sampling 34 flows) display multivectorial demagnetization behavior, and both thermal and AF treatments yield similar results (Fig. 2a). The low-coercivity (NRM to  $\sim 8$  mT) and low-temperature ( $<350$  °C) components are scattered about the present field direction and interpreted as viscous remanent magnetizations (VRM). The 150 °C step is not associated with any significant decrease in relative intensity, indicating only minor contributions from minerals of the goethite family. For peak applied fields of 40–130 mT or temperatures of 400–570 °C (Fig. 2a), the remanent direction decays linearly to the origin. The high-temperature/high-coercivity component within the lower unit varies from a NNW to NNE direction with downward inclination. Unblocking temperatures, medium- to high-coercivity components, and petrographic investigation showing the ubiquity of large, as well as small magnetite grains ( $<1$  to 5  $\mu\text{m}$ ; Background Data Set), agrees well with the main carrier of remanent magnetization being a mixture of large multidomain titanomagnetite and single and/or pseudo single-domain magnetite.

As in the lower unit, intermediate unit specimens (162 specimens from 122 cores sampling 19 flows and 1 sediment horizon) display two directional components, with directions obtained from thermal and AF demagnetization in good agreement (Fig. 2b). After removal of a low-temperature and/or low-coercivity (VRM) component, the direction decays linearly to the origin until  $\sim 130$  mT or  $\sim 560$  °C, showing NW to N declination with downward inclination. Unblocking temperatures ranging from 350 to 580 °C and high coercivity ( $\sim 40$ –100 mT) argue in favor of a main carrier of remanent magnetization being both large multidomain oxidized–exsolved titanomagnetite, as well as small pseudo single- or single-domain magnetite grains. Some specimens from the Ait Ourir section demonstrate a maghemite–hematite component, displaying an increased susceptibility upon heating between 350 and 500 °C.

In the intermediate unit sampled at the Tiourjidal and Oued Lahr sections, we found a reversed, roughly antipodal direction (Fig. 2b). These reverse

magnetizations are generally stable over a temperature range similar to those normal polarity magnetizations that attained stable endpoints (150–525 °C), suggesting the unblocking of titanomagnetite, and above 525 °C, become unstable or trend towards anomalous directions suggesting transformation of maghemite into magnetite. Due to strong overprinting by the present field, we use great circles to infer reversed polarity directions [26] and choose to not include those data whose great circles end further than 45° from the expected reversed polarity direction. At the Tiourjidal section, this reversed polarity component is found in a  $\sim 1$ -m-thick local limestone interlayer ([10], Fig. 2b) within the intermediate unit, where the upper part of the sediments are in contact with and are remagnetized by overlying pillow lava structures. A reversed direction is also observed at the Oued Lahr section, in pillow lavas just above the transition from the lower to the intermediate unit (Fig. 2b), where the top of the pillow lava flow shows partial remagnetization by the overlying, normal polarity flow. The two observed reversed polarity events occur at different relative horizons within the intermediate unit, spatially separated by over 50 km. Thus, the synchrony of these two reversed polarity events remains ambiguous.

In both the upper (136 specimens from 91 cores sampling 11 flows, Fig. 2c) and recurrent units (46 specimens from 26 cores sampling 3 flows and sediments, Fig. 2d), specimens behave similarly, displaying multivectorial components. A low-coercivity component interpreted as VRM is followed by a high-coercivity component unblocking by  $\sim 40$ –130 mT or 400–560 °C with a general NW downward direction, as before, arguing in favor of both multidomain and/or pseudo single- or single-domain magnetite grains as the primary carrier of remanent magnetization. One upper unit flow (flow 3, Jebel Imizar) shows a direction much more similar to those of the intermediate unit (Table 1). This flow was located across a faulted zone, and may have been misidentified in the field; thus, we have excluded these data from formation mean calculations. Samples from the two different sections sampling the recurrent unit (Ait Ourir and Agouim) show slightly different directions (Fig. 2d). The mean direction for the recurrent unit of the Agouim

section is similar to that of the upper unit, as is the site mean of the recurrent unit at the Ait Ourir section. The mean directions for the Agouim and Ait Ourir recurrent units, however, differ from each other by tens of degrees in declination and inclination (Table 1). The discrepancy between these outcrops separated by ~50 km may reflect the discontinuous nature of the recurrent unit, but more likely, is a result of the difficulty of determining paleohorizontal for the recurrent unit at the Ait Ourir section, where the local flow exposure was poor, and bedding orientation difficult to discern. Consequently, we also exclude the recurrent unit data of Ait Ourir from further calculations.

Mean flow directions are presented in Table 1 by sample location. Data from thin flows represented by <2 cores are not included. Mean flow directions for the lower and upper units cluster tightly, while data from the intermediate and recurrent units show a larger variation in declination. One obvious feature, best seen in the Tiourjdal section (Fig. 3) but observed in all sampled sections, is the occurrence of groups of consecutive lava flows with the same mean direction within uncertainties. We define each such directional group (DG) as a set of consecutive flows with statistically indistinguishable paleomagnetic directions where the variation of the DG is less than the  $A_{95}$  of the mean group direction, and the

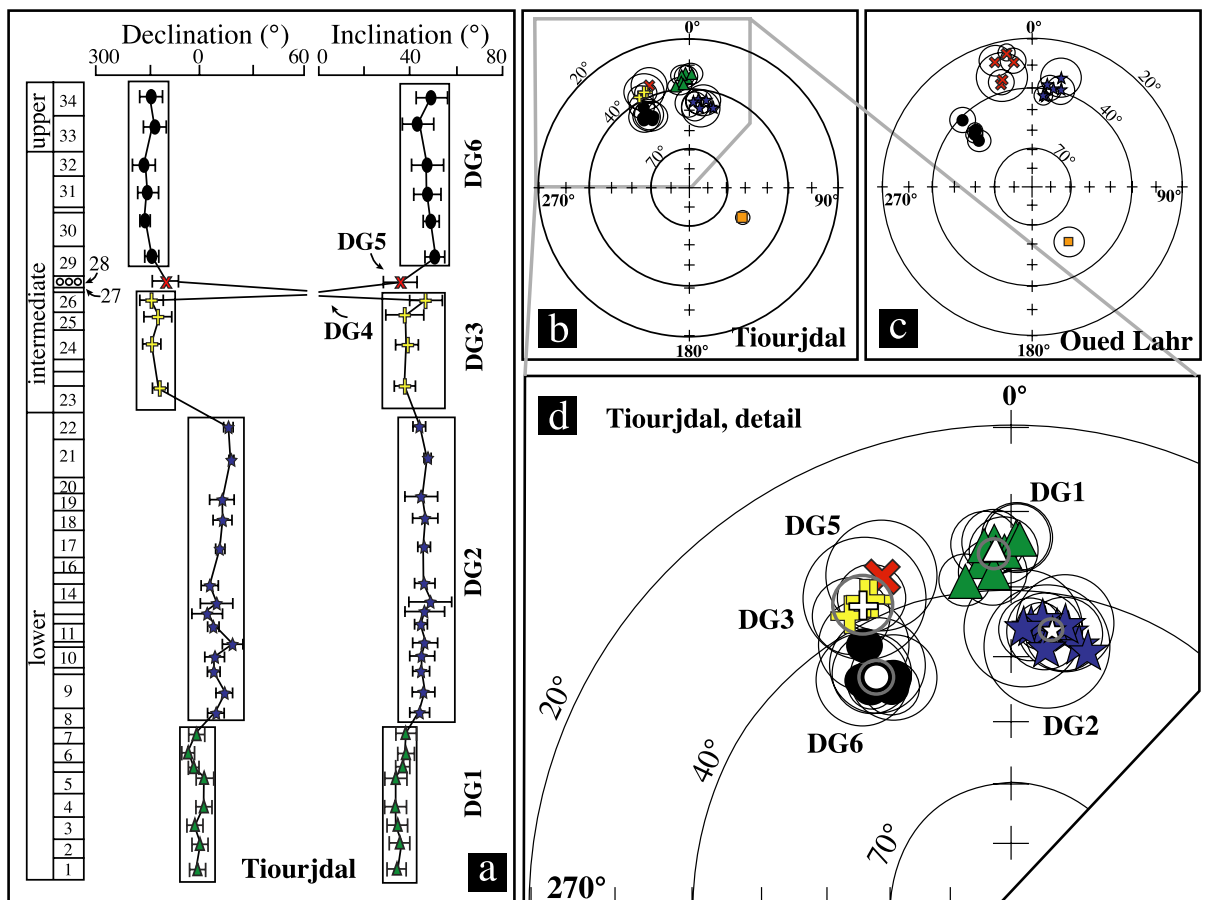


Fig. 3. (a) Magnetostratigraphy, mean flow declination, and inclination and directional groups (DGs) from the continuous Tiourjdal section are shown, as discussed in the text. (b) Projection of mean flow directions from Tiourjdal. Symbols correspond to DGs identified by single-cluster analysis of mean flow directions. (c) Projection of mean flow directions from the continuous Oued Lahr section. Symbols indicate proposed DG correlations (DG2, DG4, DG5, and DG6). Note that the basal lava flows at Oued Lahr did not outcrop and that they were not sampled. (d) Detail of Tiourjdal mean flow directions overlain with Tiourjdal DG mean directions (white symbols).

jump in the direction is greater than the mean  $A_{95}$  of the previous group. Flows within the lower unit show the presence of two directional groups, while the intermediate unit shows a wide variation in direction, with at least three identifiable groupings that overlap with both the lower unit and upper unit poles (Fig. 4). A slight offset between the Oued Lahr and Tiourjidal clusters (Fig. 3b,c) from the intermediate unit may be a result of relative rotation, but falls well within the range of intermediate unit

directions (Fig. 4). The upper unit displays more tightly clustered poles, agreeing with the much smaller volume and (inferred) briefer eruptive duration of these flows. The recurrent unit displays a similar direction to the upper unit, but the time separating eruption of these two formations is unclear. More than two thirds of the total erupted volume of Moroccan CAMP volcanism in the High Atlas seems to be contained within only three DGs, including the entire lower unit, and approximately half of the intermediate unit.

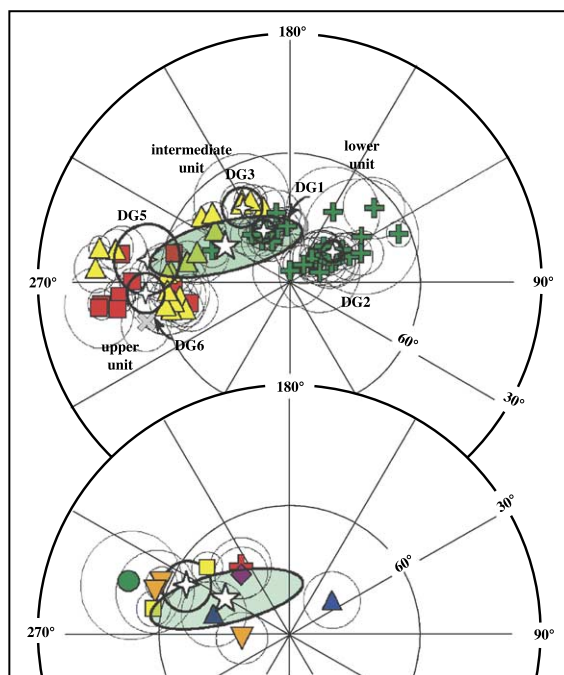


Fig. 4. VGPs determined from accepted mean site directions in this study (Table 1) plotted with  $A_{95}$  errors, overlain by mean poles (white four-point stars) from the five primary directional groups: DG1, DG2, DG3, DG5, and DG6 (Table 3). Lower unit poles shown with crosses, intermediate unit poles shown with triangles, upper unit poles shown with squares, recurrent unit pole shown (for reference) with an 'X'. The mean pole and bivariate error determined from this study is shown with a white five-point star. The lower projection displays determined paleopoles and their reported  $A_{95}$  from this and previous studies of Moroccan CAMP rocks (Table 3). Poles with  $A_{95} > 15.0$  are not plotted. Data from [28] shown by square symbols, [29] shown by a cross symbol, [30] shown by an upwards triangle, [31] shown with a downwards triangle, [32] shown with a circle, and [33] shown with a diamond. The African mean pole at 200 Ma determined by [34] is shown with a white four-point star, that from this study shown with a white five-point star.

#### 4. $^{40}\text{Ar}/^{39}\text{Ar}$ results

$\text{CO}_2$  laser incremental heating analyses of 22 plagioclase separates from 11 different flows (including one previously reported in [10]) from lavas of the High Atlas display a variety of spectra. Eight analyses with very low (<15%) radiogenic Ar contents (see Table 2) yielded unreliable results dominated by atmospheric argon, and are not discussed further. Eight of the remaining 14 analyses yielded well-defined age plateaux (Fig. 5) on a total of five lava flows. Spectra often show younger apparent ages in the lowest temperature steps as well as suppressed Ca/K ratios, a probable result of the contribution from K-rich alteration phases formed at low temperature such as sericite identified in plagioclase. The mean square of weighted deviates (MSWD) values of plateau ages from the lower through the upper units range from 0.5 to 1.2, indicating good correspondence between expected and estimated errors. Isotope correlation diagrams (isochrons) for samples yielding plateau ages indicate a trapped  $^{40}\text{Ar}/^{36}\text{Ar}$  ratio generally indistinguishable from an  $^{40}\text{Ar}/^{36}\text{Ar}$  atmospheric ratio of  $\sim 296$ . Results of all individual analyses are summarized in Table 2.

Age spectra from 14 experiments are presented from the bottom (lower unit) to the top (upper unit) of the lavas, along with the Ca/K ratio and percent of radiogenic  $^{40}\text{Ar}$  (Fig. 5). All experiments where separate grain size fractions were analyzed and yielded plateau ages are concordant at the  $2\sigma$  level (Fig. 5 and Table 2). The weighted mean of ages from samples yielding plateaux and corresponding to the same flow was used to calculate the reported age of the flow (see online appendix). All spectra obtained

Table 2  
Summary of individual  $^{40}\text{Ar}/^{39}\text{Ar}$  analyses

ID	Sample name	Unit	Location	Grain size ( $\mu\text{m}$ )	Disk	Plateau age (Ma) $\pm 2\sigma$	MSWD	$^{39}\text{Ar}$ in plateau (%)	Total gas age (Ma) $\pm 2\sigma$	Isochron age (Ma) $\pm 2\sigma$	$^{40}\text{Ar}/^{36}\text{Ar}$ intercept $\pm 2\sigma$	MSWD	Average Ca/K
33338	MOR01	low	Oued Ammasine	180–250	G	200.5 $\pm$ 1.6	0.5	88.8	200.5 $\pm$ 1.6	200.6 $\pm$ 1.8	300.3 $\pm$ 18.4	0.9	42
33340	MOR01	low	Oued Ammasine	106–180	G	200.7 $\pm$ 1.6	0.6	89.8	201.0 $\pm$ 1.6	201.2 $\pm$ 2.2	283.0 $\pm$ 55.4	1.1	42
56244	TIO01a	low	Tiourjidal	106–180	A	200.4 $\pm$ 1.4	0.8	96.1	199.8 $\pm$ 1.4	200.8 $\pm$ 1.5	278.1 $\pm$ 31.6	0.8	30
56246	TIO01a	low	Tiourjidal	180–250	A	199.7 $\pm$ 1.4	1.0	84.0	199.3 $\pm$ 1.4	200.0 $\pm$ 1.4	281.4 $\pm$ 21.0	0.4	33
56248	TIO01b	low	Tiourjidal	180–250	A	199.3 $\pm$ 1.8	3.9	89.8	198.7 $\pm$ 1.6	199.6 $\pm$ 1.4	274.7 $\pm$ 53.2	3.4	35
56250	TIO01b	low	Tiourjidal	106–180	A	199.3 $\pm$ 1.4	1.2	77.9	198.6 $\pm$ 1.4	199.7 $\pm$ 1.4	251.3 $\pm$ 54.8	1.1	35
56257	TIO03	low	Tiourjidal	106–180	B	200.1 $\pm$ 2.8	0.6	84.2	190.6 $\pm$ 2.8	197.8 $\pm$ 19.6	297.7 $\pm$ 13.8	1.2	38
56267	TIO03	low	Tiourjidal	180–250	B	201.2 $\pm$ 2.4			201.2 $\pm$ 2.4	232.9 $\pm$ 5.6	287.1 $\pm$ 1.4	2.7	32
33332	MOR04a	int	Ait Ourir	106–180	G	200.9 $\pm$ 2.4	0.3	41.6	192.7 $\pm$ 1.8	199.7 $\pm$ 4.4	306.1 $\pm$ 31.6	0.3	87
33336	MOR04a	int	Ait Ourir	180–250	G	199.3 $\pm$ 2.2	0.6	44.2	202.6 $\pm$ 2.0	199.9 $\pm$ 2.4	307.1 $\pm$ 12.8	1.8	91
33335	MOR04b	int	Ait Ourir	106–180	G	209.4 $\pm$ 3.6			209.4 $\pm$ 3.6	197.5 $\pm$ 18.9	299.4 $\pm$ 2.8	1.6	79
33343	MOR04b	int	Ait Ourir	180–250	G	326.0 $\pm$ 12.7			326.0 $\pm$ 12.7	161.0 $\pm$ 27.4	297.8 $\pm$ 1.2	3.4	74
56259	TIO04	int	Tiourjidal	180–250	B	189.8 $\pm$ 4.0			189.8 $\pm$ 4.0	214.5 $\pm$ 9.3	294.4 $\pm$ 1.6	1.2	66
56261	TIO04	int	Tiourjidal	106–180	B	224.6 $\pm$ 7.8			224.6 $\pm$ 7.8	248.5 $\pm$ 19.2	297.6 $\pm$ 1.4	5.8	70
56263	TIO05	int	Tiourjidal	180–250	B	199.7 $\pm$ 1.6	0.8	73.4	195.3 $\pm$ 1.6	200.7 $\pm$ 2.0	252.9 $\pm$ 33.9	0.4	70
56265	TIO05	int	Tiourjidal	106–180	B	199.2 $\pm$ 1.6	1.9	62.1	195.2 $\pm$ 1.6	200.3 $\pm$ 2.2	261.8 $\pm$ 48.2	1.8	63
33330	MOR05	upp	Ait Ourir	180–250	G	230.9 $\pm$ 4.8			230.9 $\pm$ 4.8	225.7 $\pm$ 16.2	296.5 $\pm$ 2.0	3.8	106
33342	MOR05	upp	Ait Ourir	106–180	G	469.0 $\pm$ 20.0			469.0 $\pm$ 20.0	284.9 $\pm$ 51.2	300.8 $\pm$ 1.6	3.4	68
33350	MOR08	upp	Jebel Imizar	106–180	H	178.4 $\pm$ 3.4			178.4 $\pm$ 3.4	148.1 $\pm$ 2.6	302.8 $\pm$ 0.8	4.0	66
33361	MOR08	upp	Jebel Imizar	180–250	H	238 $\pm$ 8.1			238 $\pm$ 8.1	167.7 $\pm$ 25.8	302.1 $\pm$ 4.8	3.2	91
33351*	MOR14	upp	Oued Lahr	106–180	H	199.8 $\pm$ 1.8	0.5	88.0	198.1 $\pm$ 2.4	201.1 $\pm$ 3.0	295.0 $\pm$ 1.4	0.5	125
33362	MOR14	upp	Oued Lahr	180–250	H	222.3 $\pm$ 4.5			222.3 $\pm$ 4.5	193.3 $\pm$ 9.1	295.5 $\pm$ 1.0	3.8	114

Ages are calculated relative to FC sanidine (28.02 Ma [20]), with accepted plateau ages shown in **bold** type. Errors are provided at  $2\sigma$  unless otherwise noted, and reflect uncertainties in isotope measurements, corrections for reactor-induced interferences and neutron fluence ( $J$ ). Degassing diagrams for samples with  $<15\%$   $^{40}\text{Ar}^*$  are shown in italics and are not provided (Fig. 5), but may be referred to in the on-line data table. Plateau ages in italics are shown for reference, only, and are not accepted ages, as discussed in text. \*MOR14 33351 age originally reported in [10].

from the lower unit are statistically indistinguishable, yielding six plateau ages ranging from  $200.7 \pm 1.6$  to  $199.3 \pm 1.4$  Ma (Fig. 5) with similar behavior and lower average Ca/K ratios of  $\sim 35$ . One sample, the larger grain size of TIO01b, shows a large amount of scatter outside of expected errors (MSWD=3.9), and is not considered a plateau age, although the determined age of  $199.3 \pm 1.8$  Ma is indistinguishable from the plateau yielded by the smaller grain size fraction ( $199.3 \pm 1.4$  Ma), with an MSWD of 1.2. The weighted mean age of the lower unit lavas is  $200.1 \pm 0.6$  Ma.

Samples from the intermediate unit display a large range of average Ca/K ratios (30–90) and notably more disturbed spectra. This behavior is often correlated with low radiogenic argon ( $^{40}\text{Ar}^*$ ) contents contributing only 3–40% to the total  $^{40}\text{Ar}$ , and higher more variable Ca/K ratios. The result is a dramatic increase in the relative error due to low  $^{40}\text{Ar}^*$  content and large corrections on calcium derived argon isotopes. All eight analyses from the intermediate unit are less precise, and yield only one age fitting our plateau criteria, of  $199.7 \pm 1.6$  Ma (MSWD=0.8). A second grain size analyzed from the same flow yields a similar age ( $199.2 \pm 1.6$  Ma), but with an excess scatter (MSWD=1.9), and is thus rejected. Only one spectrum was obtained for an upper unit lava, which yielded a plateau age of  $199.8 \pm 1.8$  Ma [10]. This age is slightly younger than those obtained for the lower unit, but statistically indistinguishable at the  $2\sigma$  level from all other determined ages within this study, confirming a rapid mean eruption rate. The weighted mean age of all CAMP lavas presented in this study is  $199.9 \pm 0.5$  Ma.

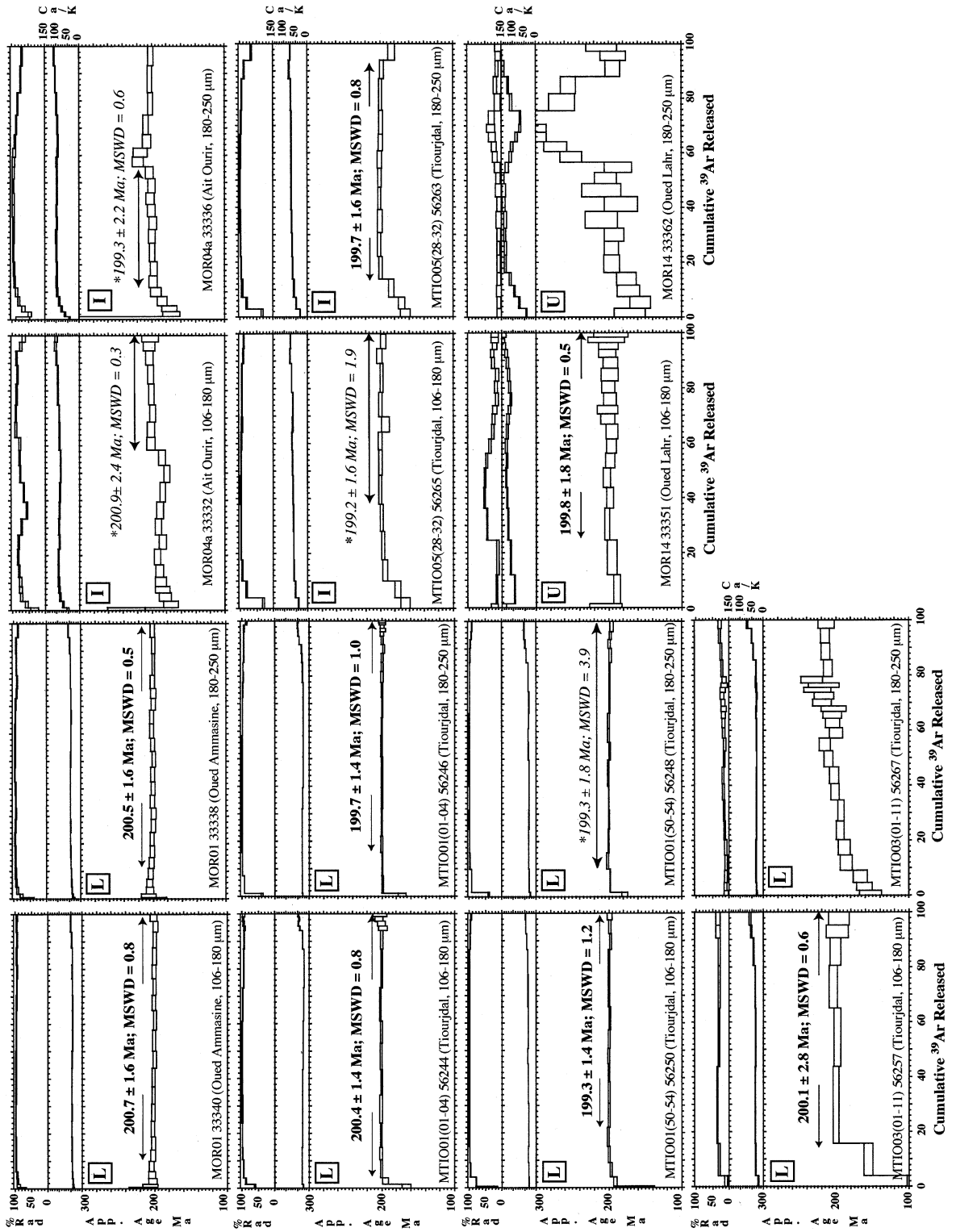
## 5. The tempo of Moroccan CAMP volcanism

We have compiled all available  $^{40}\text{Ar}/^{39}\text{Ar}$  plateau ages from the literature (see online appendix) including our new ages, recalculated where necessary to reflect the same monitor age (Fish Canyon sanidine, 28.02 Ma [20]), and present them as an age probability diagram (Fig. 6). Application of a quality filter, choosing only data which come from samples including  $>70\%$   $^{39}\text{Ar}$  from a determined plateau and showing no obvious slope or disturbance, has reduced artifacts due to alteration, recoil, and excess argon, all

of which tend to increase dispersion of the data. Rigorous treatment of the available  $^{40}\text{Ar}/^{39}\text{Ar}$  age data results in a very narrow window of time focused on a major magmatic event initiating at  $\sim 200$  Ma and possibly continuing in minor amounts until  $\sim 192$  Ma. The filter we have applied obviously does not ensure exclusion of spurious ages and further scrutiny of outliers would be useful.

Ages constraining the bulk of the Moroccan volcanism place CAMP volcanism in Morocco at the peak of this magmatic event, and emphasize the brevity of the event. Our compilation also illustrates that the dating of CAMP volcanism in Morocco is now far better constrained (Fig. 6), and therefore overrepresented, compared to other occurrences of CAMP-related magmatism. Two locations (the lava flows of Morocco and the Fouta Djallon sill in Guinea) contribute over 75% of the accepted age data for the Central Atlantic Magmatic Province. To piece together the evolution and overall timing of the CAMP, further chronologies study in other parts of the province is warranted. Present data affirm that the maximum eruptive duration of the main pulse of volcanism is  $<2$  Ma in Morocco, with no detectable variation in age within  $2\sigma$  errors between the lower and upper unit. A minimum duration, however, is difficult to estimate from radioisotopic age data alone due to the typical age uncertainty of  $\pm \sim 0.5$ –1%, even neglecting systematic errors.

In flood basalts, rapid episodic direction changes are most likely the result of an eruption rate that was rapid relative to the rate of secular variation [35,36]. Paleomagnetic data, as well as the presence of sediments between the various formations suggest the division of Moroccan CAMP volcanism into several pulses. We have identified at least four primary directional groups and one magnetic polarity reversal, present in the Tiourjald section, and supported by the magnetic declination and inclination data from the other sections in this study (Fig. 3 and Table 1). Previous paleomagnetic studies of CAMP volcanics have been noted in several cases to reveal dispersed directions [e.g., [31]], often been attributed to indicate a wider (and younger) range of remanence ages [37–39]. We find no evidence of age variation within the Moroccan lavas, however, based on our  $^{40}\text{Ar}/^{39}\text{Ar}$  age results. Variable paleohorizontal orientations can also be ruled out as these variations are



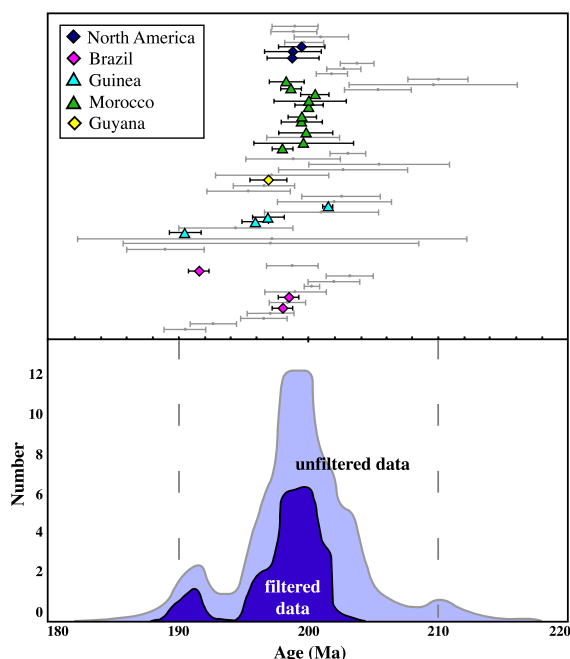


Fig. 6. Comparison of filtered published  $^{40}\text{Ar}/^{39}\text{Ar}$  plateau ages and reported  $2\sigma$  errors on CAMP volcanic and intrusive activity. Age probability diagram uses 1 Ma bins, shaded areas compare the filtered and unfiltered  $^{40}\text{Ar}/^{39}\text{Ar}$  plateau age data sets. Accepted western Atlantic margin ages (North America, Brazil, and Guyana) shown with diamonds, eastern Atlantic margin ages (Morocco and Guinea) shown with triangles. Rejected ages are shown with grey dots. All ages shown are listed in the Background Data Set.

well constrained for most sections (Background Data Set), and are negligible for the Tiourjdal section. DGs are defined by changes in inclination as well as in declination, with a maximum variation in Tiourjdal ( $\text{var}_D=44^\circ\pm 42^\circ$ ;  $\text{var}_I=17^\circ\pm 9^\circ$ ) that agrees within error with the expected general variation ( $15^\circ\pm 5^\circ$ ) for the considered paleolatitude [40]. The general correspondence of CAMP eruptive units (identified based on field observation and geochemistry [10]) with our suggested directional groups is consistent with a picture of punctuated eruption. Our data confirm this eruptive mode and highlight the episodic nature of CAMP volcanism.

The presence of directional groups indicates brief pulses of lavas, generally within the maximum age resolution presently possible from  $^{40}\text{Ar}/^{39}\text{Ar}$  dating methods, that do not completely average secular variation. Similar findings within the North Atlantic Tertiary Province [41] suggest that spot recordings of secular variation may be typical of the nature of rapidly erupted large igneous province volcanism. Accordingly, dense sampling over the entire stratigraphic succession of lavas and identification of directional groups is likely necessary to adequately average secular variation for any large igneous province. It follows that brief volcanic pulses and directional groups present a potentially useful tool for temporal correlation of flows and intrusives across the North African CAMP province, as well as across other large igneous provinces (e.g., [42]).

Each DG record displays smaller variation both in  $\text{VGP}_{\text{long}}$  and  $\text{VGP}_{\text{lat}}$  (Table 3) than that observed over a 450-year period in the late Holocene (maximum  $\text{VGP}_{\text{lat}}$  variation of  $7.8^\circ$ ; [43]). Assuming that paleosecular variation at 200 Ma was of similar amplitude to that of the Holocene, each individual DG cluster may correspond with a volcanic event of very short duration, possibly  $\ll 450$  years. Approximately five volcanic pulses with distinct clustered directions and the presence of at least one polarity reversal (1000–8000 years [44]) within the lava pile provides a lower estimate on the duration of volcanism of  $<20$  kyr. We cannot infer the time gap between each volcanic pulse, however, which could plausibly be thousands of years or more. Our maximum ( $^{40}\text{Ar}/^{39}\text{Ar}$ ) and minimum (secular variation) estimates compare well with a proposed duration of  $\sim 580$  kyr in the northeastern United States [5], where only the youngest CAMP lavas (the Orange Mtn. through Hook Mtn. Basalt, corresponding to the intermediate/upper units and recurrent unit, respectively [10]) are present.

Several paleomagnetic studies in Morocco focused on CAMP-related rocks [28–33] in the 1970s, well before the extent and age of CAMP was recognized. These studies generally relied on end-vector point

Fig. 5.  $^{40}\text{Ar}/^{39}\text{Ar}$  apparent age spectra, Ca/K ratios, and percentage of radiogenic  $^{40}\text{Ar}$  from 14-step heating experiments on plagioclase separates from CAMP lava flows. 'L': lower unit; 'I': intermediate unit lava; 'U': upper unit lava. Plateau ages with  $2\sigma$  uncertainties include uncertainty from isotope measurements and interference corrections. Ages with asterisks are shown for comparison only, and are not accepted, as discussed in the text.

Table 3  
Paleomagnetic poles from Moroccan CAMP lithologies

Directional group mean poles	<i>N</i>	VGP <sub>lat</sub>	VGP <sub>long</sub>	<i>k</i>	<i>A</i> <sub>95</sub>
Paleomagnetic data, CAMP-related sediments and lavas (this study)					
DG1 lava flows	12	77.2	207.1	257	2.7
DG2 lava flows	23	78.1	125.4	145	2.5
DG3 lava flows	7	56.6	261.1	60	7.8
DG5 lava flows	5	69.7	212.4	272	4.6
DG6 lava flows	14	56.6	274.7	84	4.4
200 Ma African mean directional group paleomagnetic pole (this study)					
5	73.0	241.3	5.0	18.5	Dm
Paleomagnetic data from other studies of Moroccan CAMP-related sediments, lavas and intrusives					
		<i>N</i>	VGP <sub>lat</sub>	VGP <sub>long</sub>	<i>A</i> <sub>95</sub>
Hailwood and Mitchell [28]	Draa Valley sills	16	65.5	230.5	3.5
Hailwood and Mitchell [28]	Foum-Zguid dike	5	58.0	259.0	4.0
Bardon et al. [29]	Moroccan volcanics	27	71.0	216.0	7.0
Hailwood [30]	Issaldain dolerites	8	77.5	129.5	6.5
Hailwood [30]	Ait Aadel dolerites	15	72.0	254.5	7.5
Hailwood [30]	<i>Titchka sediments</i>	4	68.5	267.0	22.5
Daly and Pozzi [31]	Khénifra basalts	9	58.1	248.0	3.7
Daly and Pozzi [31]	Beni-Snassen basalts	12	57.4	252.0	9.2
Daly and Pozzi [31]	Tazzeke basalts	6	79.1	274.2	5.9
Martin et al. [32]	<i>Telouet lava</i>	1	51.4	215.6	16.0
Martin et al. [32]	Argana Redbeds	22	50.6	251.4	12.0
Westphal et al. [33]	Upper 'Triassic'	34	72.0	218.0	6.0

Paleomagnetic virtual geomagnetic pole determinations from CAMP-related lavas, intrusives and sediments in Morocco (this study and [28–33]). Mean directional group paleomagnetic pole does not incorporate reversed flows (DG4), nor DG7 (see text). Rock associations to CAMP are based on our reevaluation of published descriptions, map locations and poles. Poles with  $\alpha_{95} > 15.0$  are shown in italics and are not plotted (Fig. 4).

analysis and, in most cases, only one demagnetization step. Additionally, studies sometimes mix CAMP-related rocks with those of other ages and associations, which we have tried to exclude. Reversed polarities are occasionally reported, but the context and temporal association of samples is not always clear (e.g., [33]). Comparison with previous paleomagnetic studies and reevaluation of data reported from Moroccan lava flows, sills, dikes, and sediments of Triassic–Jurassic age in the context of our findings (Table 3) is not always straightforward, but the representation of various directional groups throughout these studies is clear (Fig. 4). The mean pole for Moroccan CAMP calculated using mean flow poles from 66 flows and sediments from all sampled sections (Table 1) is  $\lambda(^{\circ}\text{N})=77.2^{\circ}$ ,  $\phi(^{\circ}\text{E})=240.9^{\circ}$  ( $A_{95}=4.6^{\circ}$ ), distinct from the expected 200 Ma pole

for Africa of  $\lambda(^{\circ}\text{N})=63.9^{\circ}$ ,  $\phi(^{\circ}\text{E})=244.6^{\circ}$  ( $A_{95}=5.7^{\circ}$ ) [34], as might be expected in light of the presence of rapid eruptive pulses. Despite including only consistently analyzed and densely sampled data directly tied to radioisotope age constraints, our data do not adequately sample secular variation, and, therefore, our determined mean pole does not by itself represent a mean 200 Ma African pole. Our DGs should be sufficiently dispersed to average secular variation, however, without overrepresentation of any given group. We exclude DG7 from the recurrent unit of unconfirmed age, and DG4 from the reversed layers represented by single flows, which may comprise one or two events. The DG distribution is not fisherian, and, therefore, errors are better evaluated with bivariate [45] statistics. Taking the mean pole determined from our five DG poles (Table 3) yields

an African pole for 200 Ma of  $\lambda(^{\circ}\text{N})=73.0^{\circ}$ ,  $\phi(^{\circ}\text{E})=241.3^{\circ}$  ( $D_p=5.0^{\circ}$ ,  $D_m=18.5^{\circ}$ ), indistinguishable from that of [34] (Fig. 4).

## 6. CAMP and Triassic–Jurassic boundary

The Triassic–Jurassic (Tr/J) boundary is often considered among the most significant mass extinctions in the last 0.5 Ga, with some studies estimating 80% of species lost [46], comparable to the Cretaceous–Tertiary (K/T) extinction ca. 65 Ma. Recent review of the extinction record [16], however, shows that much work remains to be done to clarify the tempo and extent of this extinction event. The Tr/J boundary is best defined in the marine record, generally by ammonoid biostratigraphy. The terrestrial Tr/J boundary record is currently best constrained by palynoflora zones, despite some concerns with the reliability of pollen and spore dispersion in the biostratigraphic record. Correlation between the marine and terrestrial record is imperfect, at best, and this study provides one possible means of correlation through paleomagnetic correspondence.

Magnetostratigraphic work on a terrestrial section across the Triassic–Jurassic boundary preserved in the Newark Basin (eastern North America) [47], which includes CAMP lava flows, identifies a minor reversal in the Martinsville section (renamed E23r; [48]). This brief reversal, identified in 2 specimens, occurs in sediments ~20m below the lowest lavas present at this section (the Orange Mountain Basalts), which share a strong geochemical correlation with the Moroccan upper unit [10]. Plagioclase separates from the Orange Mountain Basalts are dated at  $201.0 \pm 2.1$  Ma [49] by an age spectrum showing some disturbance, but are contemporaneous within errors with our ages for the CAMP lavas of Morocco. Observation and geochemical evidence [10] indicate that some portion of the intermediate unit and the entire lower unit are absent in the Newark Basin. Based on these multiple lines of evidence, the observed reversals within the intermediate unit are tentatively correlated to the E23n, E23r, E24n sequence seen in the Newark Basin. Magnetostratigraphy has also been reported from a drill core from the Triassic–Jurassic

Paris Basin [50] showing the presence of two brief reversals, although the youngest is identified by a single sample, and the work is not tied into an absolute timescale.

Results reported from the Triassic–Jurassic marine section at St. Audrie’s Bay (United Kingdom) [19] identify a brief set of reversals (SA5.2r, .3r, and SA5r) in successive horizons, occurring just before and within the Triassic–Jurassic transition, also tentatively correlated with E23r of the Newark Basin. This transition zone in St. Audrie’s Bay occurs after the last appearance of late Triassic conodonts and before the first occurrence of Jurassic ammonoids. A correlative section tentatively linking the St. Audrie’s Bay marine section with the Newark Basin and the Moroccan CAMP lavas is shown (Fig. 7), and suggests that volcanism commenced well before the proposed boundary age in marine sediments, as has been inferred from multiple other lines of evidence [10,51].

Other hypotheses relating to the cause of the Tr/J mass extinction include a moderate iridium enrichment above the Tr/J palynoflora limit, in the Jacksonwalt syncline, associated with a small fern spike [52]. The enrichment has an averaged maximum of 144 ppt, more than an order of magnitude smaller than that reported at the K/T boundary of ~3000 ppt [53]. Our paleomagnetic and  $^{40}\text{Ar}/^{39}\text{Ar}$  ages imply that the inferred Ir anomaly hypothesized to be related to an impact having a causal relationship to the Tr/J boundary extinction must postdate the onset of volcanism.

The age of the Tr/J boundary and extinction was recently reevaluated using the U/Pb zircon method by Pálffy and collaborators [54,55] in a tuff interstratified in marine sediments, occurring slightly (~3.5m) below the boundary at  $199.6 \pm 0.3$  Ma. This age was determined from multigrain zircon fractions, which can bias the age due to unrecognized lead loss and/or older inheritance [56]. On closer view, these eight multigrain analyses show very complex behavior, with five of the eight analyses not yielding the suggested age. Taking into account the recently inferred 1% to 1.5% bias between U/Pb and K/Ar dating systems [57,58], most of the published  $^{40}\text{Ar}/^{39}\text{Ar}$  ages in Morocco are marginally older (within analytical errors) than the minimum age for the Tr/J extinction [55], but cannot be currently resolved from the Triassic–Jurassic boundary age.

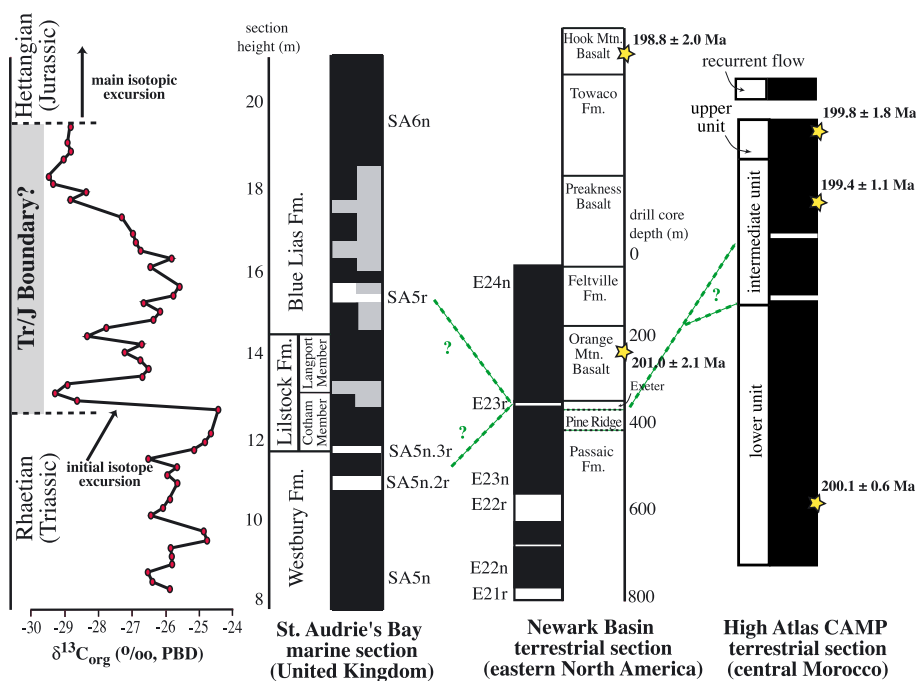


Fig. 7. Proposed correlation of Moroccan CAMP magnetostratigraphy and ages. Lower and intermediate unit ages shown are weighted mean formation ages presented in this paper; the age of the upper unit is from [10]. Data compared with paleomagnetic data from the terrestrial Martinsville drill core of the Newark Basin [47,48], using ages of [49], as well magnetostratigraphy [19], lithostratigraphy, and  $\delta^{13}\text{C}$  isotopic data [13] of the St. Audrie's Bay marine section. The vertical axes of the three sections are not scaled relative to one another.

Magnetostratigraphic results suggest that more than half the volume of CAMP lavas in Morocco (the lower unit and part of the intermediate unit) were erupted before a brief period of reversed magnetic polarity (E23r, Fig. 3), which preceded the Tr/J boundary extinction. Paleomagnetic data reveal a pulsing eruptive mode, with several large-volume and short-lived volcanic pulses (possibly  $\leq 0.4$  kyr) occurring during this major volcanic event. An eruption rate modulated by brief pulses of intense volcanism has the potential to introduce considerable quantities of volatiles into the atmosphere over rapid time periods, and contrasted with a model assuming constant extrusion rates, may have played a crucial role in driving the events of the Tr/J boundary (e.g., [4,13,15]).

## Acknowledgments

The authors extend sincere thanks to the entire field team that made this study possible: G. Bellieni, H. Ibouh, J. Madeira, R. Martini, F. Medina, C.

Rapaille, C. Verati, L. Zaninetti, K. Allenbach and R. Neuwerth, and our driver, Driss. We gratefully acknowledge the constructive reviews of P. Riisager and an anonymous reviewer, as well as candid discussions of data and ideas with R. Coe, J. Glen, M. Hounslow, J. Lyons, R. Mundil, and G. Scott. We thank T. Teague and J. Runnoe for assistance with sample preparation and laboratory work. This study was supported by NSF grant EAR-9909517 to PRR, Moroccan PARS (SDU-30) to NY and the Swiss FNRS (2000-064580.01) to AM.

## Appendix A. Background data set

Supplementary data associated with this article can be found, in the online version, at [doi:10.1016/j.epsl.2004.09.022](https://doi.org/10.1016/j.epsl.2004.09.022).

## References

- [1] A. Marzoli, P.R. Renne, E.M. Piccirillo, M. Ernesto, G. Bellieni, A. De Min, Extensive 200 million-year-old con-

- tinental flood basalts of the Central Atlantic Magmatic Province, *Science* 284 (1999) 616–618.
- [2] D. Reyre, Remarques sur l'origine et l'évolution des bassins sédimentaires africains de la côte atlantique, *Bull. Soc. Géol. Fr.* 26 (1984) 1041–1059.
- [3] C.R. Scotese, L.M. Gahagan, R.L. Larson, Plate tectonic reconstructions of the Cretaceous and Cenozoic ocean basins, Mesozoic and Cenozoic Plate Reconstructions, (1989) 27–48.
- [4] J.G. McHone, Volatile emissions of Central Atlantic Magmatic Province basalts: mass assumptions and environmental consequences, The Central Atlantic Magmatic Province, *AGU Geophys. Monogr.* 136 (2003) 241–254.
- [5] P.E. Olsen, R.W. Schlische, M.S. Fedosh, 580 Ky duration of the early Jurassic flood basalt event in eastern North America estimated using Milankovitch cyclostratigraphy, *Bull. Mus. North. Ariz.* 60 (1996) 11–22.
- [6] P. Le Roy, A. Piqué, Triassic–Liassic Western Moroccan synrift basins in relation to the Central Atlantic opening, *Mar. Geol.* 172 (2001) 359–381.
- [7] F. Medina, Superimposed extensional tectonics in the Argana Triassic formations (Morocco), related to the early rifting of the Central Atlantic, *Geol. Mag.* 128 (1991) 525–536.
- [8] H. Bertrand, The Mesozoic tholeiitic province of Northwest Africa: a volcano–tectonic record of the early opening of Central Atlantic, Magmatism in Extensional Structural Settings: the Phanerozoic African Plate (1991) 147–188.
- [9] H. Bertrand, J. Dostal, C. Dupuy, Geochemistry of Early Mesozoic tholeiites from Morocco, *Earth Planet. Sci. Lett.* 58 (1982) 225–239.
- [10] A. Marzoli, H. Bertrand, K.B. Knight, S. Cirilli, C. Vèrati, S. Nomade, R. Martini, N. Youbi, K. Allenbach, R. Neuwerth, N. Buratti, C. Rapaïlle, L. Zaninetti, G. Bellieni and P.R. Renne, Synchrony of the Central Atlantic Magmatic Province and the Triassic–Jurassic boundary climatic and biotic crisis, *Geol. in press*.
- [11] V. Courtillot, J.J. Jaeger, Z. Yang, G. Féraud, C. Hoffmann, The influence of continental flood basalts on mass extinctions: where do we stand? *Spec. Pap. Geol. Soc. Am. Spec. Pap.* 307 (1996) 513–525.
- [12] V.E. Courtillot, P.R. Renne, On the ages of flood basalt events, *C. R. Geosci.* 335 (2003) 113–140.
- [13] S.P. Hesselbo, S.A. Robison, F. Surlyk, S. Piasecki, Terrestrial and marine extinction at the Triassic–Jurassic boundary synchronized with major carbon-cycle perturbation: a link to initiation of massive volcanism? *Geology* 30 (2002) 251–254.
- [14] P.E. Olsen, D.V. Kent, M. Et-Touhami, J. Puffer, Cyclo-, magneto-, and bio-stratigraphic constraints on the duration of the CAMP event and its relationship to the Triassic–Jurassic boundary, The Central Atlantic Magmatic Province, *AGU Geophys. Monogr.*, 136 (2003) 7–32.
- [15] J. Pálfy, Volcanism of the Central Atlantic Magmatic Province as a potential driving force in the end-Triassic mass extinction, The Central Atlantic Magmatic Province, *AGU Geophys. Monogr.* 136 (2003) 255–267.
- [16] L.H. Tanner, S.G. Lucas, M.G. Chapman, Assessing the record and causes of Late Triassic extinctions, *Earth Sci. Rev.* 65 (2004) 103–139.
- [17] S.J. Fowell, P.E. Olsen, Time calibration of Triassic/Jurassic microfossil turnover, eastern North America, *Tectonophysics* 222 (1993) 361–369.
- [18] S.J. Fowell, A. Traverse, Palynology and age of the upper Blomidon Formation, Fundy Basin, Nova Scotia, *Rev. Palaeobot. Palynol.* 86 (1995) 211–233.
- [19] M.W. Hounslow, P.E. Posen, G. Warrington, Magnetostratigraphy and biostratigraphy of the Upper Triassic and lowermost Jurassic succession, St. Audrie's Bay, U.K., *Paleogeogr. Paleoclim. Paleocol.* 213 (2004) 331–358.
- [20] P.R. Renne, C.C. Swisher, A.L. Deino, D.B. Karner, T.L. Owens, D.J. DePaolo, Intercalibration of standards, absolute ages and uncertainties in  $^{40}\text{Ar}/^{39}\text{Ar}$  dating, *Chem. Geol.* 145 (1998) 117–152.
- [21] R.H. Steiger, E. Jäger, Subcommission on geochronology: convention on the use of decay constants in geo- and cosmochronology, *Earth Planet. Sci. Lett.* 36 (1977) 359–362.
- [22] K.B. Knight, P.R. Renne, A. Halkett, N. White,  $^{40}\text{Ar}/^{39}\text{Ar}$  dating of the Rajahmundry Traps, Eastern India and their relationship to the Deccan Traps, *Earth Planet. Sci. Lett.* 208 (2003) 85–99.
- [23] J.P. Cogné, PaleoMac: A Macintosh Application for Treating Paleomagnetic Data and Making Plate Reconstructions, *Geochem. Geophys. Geosyst.* 4 (2003) DOI:10.1029/2001GC000227.
- [24] J.D.A. Zijderveld, A.C. demagnetisation of rocks: analysis of results, *Methods in Palaeomagnetism* (1967) 254–286.
- [25] J.L. Kirshvink, The least-squares line and plane and the analysis of paleomagnetic data, *Geophys. J. R. Astron. Soc.* 62 (1980) 699–718.
- [26] T.C. Onstott, Application of the Bingham distribution function in paleomagnetic studies, *J. Geophys. Res.* 85 (1980) 1500–1510.
- [27] S.R. Fisher, Dispersion on a sphere, *Proc. R. Soc. Ser. A* 217 (1953) 2295–2305.
- [28] E.A. Hailwood, J.G. Mitchell, Palaeomagnetic and radiometric dating results from Jurassic intrusions in South Morocco, *Geophys. J. R. Astron. Soc.* 24 (1971) 351–364.
- [29] C. Bardon, A. Bossert, R. Hamzeh, M. Westphal, Etude paléomagnétique de formations du Trias et du Jurassique du Maroc et du Sahara, *C. R. Acad. Sci. Paris* 276 (1973) 2357–2360.
- [30] E.A. Hailwood, The palaeomagnetism of Triassic and cretaceous rocks from Morocco, *Geophys. J. R. Astron. Soc.* 41 (1975) 219–235.
- [31] L. Daly, J.-P. Pozzi, Résultats paléomagnétiques du permien inférieur et du trias Marocain; comparaison avec les données Africaines et Sud Américaines, *Earth Planet. Sci. Lett.* 29 (1976) 71–80.
- [32] D.L. Martin, A.E.M. Nairn, H.C. Noltimier, M.H. Petty, T.J. Schmitt, Paleozoic and Mesozoic paleomagnetic results from Morocco, *Tectonophysics* 44 (1978) 91–114.
- [33] M. Westphal, R. Montigny, R. Thuizat, C. Bardon, A. Bossert, R. Hamzeh, Paléomagnétisme et datation du volcanisme

- permien, triasique et crétacé du Maroc, *Can. J. Earth Sci.* 16 (1979) 2150–2164.
- [34] J. Besse, V. Courtillot, Apparent and true polar wander and the geometry of the geomagnetic field over the last 200 Myr, *J. Geophys. Res.* 107 (2002).
- [35] E.A. Mankinen, M. Prévot, C.S. Grommé, R.S. Coe, The Steens Mountain (Oregon) geomagnetic polarity transition: 1. Directional history, duration of episodes, and rock magnetism, *J. Geophys. Res.* 90 (1985) 10393–10416.
- [36] J. Riisager, P. Riisager, A.K. Pedersen, The C27n–C27r geomagnetic polarity reversal recorded in the west Greenland flood basalt province: how complex is the transitional field? *J. Geophys. Res.* 108 (2003) EPM4 1–EPM4 11.
- [37] S. Nomade, H. Théveniaut, Y. Chen, A. Poulet, C. Rigollet, Paleomagnetic study of French Guyana Early Jurassic dolerites: hypothesis of a multistage magmatic event, *Earth Planet. Sci. Lett.* 184 (2000) 155–168.
- [38] M. Ernesto, G. Bellieni, E.M. Piccirillo, L.S. Marques, A. de Min, I.G. Pacca, G. Martins, J.W.P. Macedo, Paleomagnetic and geochemical constraints on the timing and duration of the CAMP activity in northeastern Brazil, The Central Atlantic Magmatic Province, *AGU Geophys. Monogr.* 136 (2003) 129–149.
- [39] A. De Min, E.M. Piccirillo, A. Marzoli, G. Bellieni, P.R. Renne, M. Ernesto, L.S. Marques, The Central Atlantic Magmatic Province (CAMP) in Brazil: petrology, geochemistry,  $^{40}\text{Ar}/^{39}\text{Ar}$  ages, paleomagnetism and geodynamic implications, The Central Atlantic Magmatic Province, *AGU Geophys. Monogr.* 136 (2003) 91–128.
- [40] P.L. McFadden, R.T. Merrill, M.W. McElhinny, S. Lee, Reversals of the Earth's magnetic field and temporal variations of the dynamo families, *J. Geophys. Res.*, B 96 (1991) 3923–3933.
- [41] J. Riisager, P. Riisager, A.K. Pedersen, Paleomagnetism of large igneous provinces: case-study from West Greenland, North Atlantic igneous province, *Earth Planet. Sci. Lett.* 214 (2003) 409–425.
- [42] S.W. Bogue, R.S. Coe, Paleomagnetic correlation of Columbia River Basalt flows using secular variation, *J. Geophys. Res.* 86 (1981) 11883–11897.
- [43] E. Schnepf, R. Pucher, C. Goedicke, A. Manzano, U. Müller, P. Lanos, Paleomagnetic directions and thermoluminescence dating from a bread oven-floor sequence in Lübeck (Germany): a record of 450 years of geomagnetic secular variation, *J. Geophys. Res.* 108 (2003) 1–14.
- [44] R.T. Merrill, L.P. McFadden, Geomagnetic polarity reversals, *Rev. Geophys.* 37 (1999) 201–226.
- [45] M. LeGoff, Lissage et limites d'incertitude des courbes de migration polaire: pondération des données et extension bivariate de la statistique de Fisher, *C.R. Acad. Sci. Paris* 311 (1990) 1191–1198.
- [46] J.J. Sepkoski Jr., Patterns of Phanerozoic extinction: a perspective from global data bases, *Global Events and Event Stratigraphy in the Phanerozoic*, 1996, pp. 35–51.
- [47] D.V. Kent, P.E. Olsen, W.K. Witte, Late Triassic–earliest Jurassic geomagnetic polarity sequence and paleolatitudes from drill cores in the Newark Rift Basin, eastern North America, *J. Geophys. Res.* 100 (1995) 14965–14998.
- [48] D.V. Kent, P.E. Olsen, Astronomically tuned geomagnetic polarity time scale for the Late Triassic, *J. Geophys. Res.* 104 (1999) 12831–12841.
- [49] W.E. Hames, P.R. Renne, C. Ruppel, New evidence for geologically instantaneous emplacement of earliest Jurassic Central Atlantic Magmatic Province basalts on the North American margin, *Geology* 28 (2000) 859–862.
- [50] Z. Yang, M.-G. Moreau, H. Bucher, J.-L. Dommergues, A. Trouiller, Hettangian and Sinemurian magnetostratigraphy from Paris Basin, *J. Geophys. Res.* 101 (1996) 8025–8042.
- [51] A.S. Cohen, A.L. Coe, New geochemical evidence for the onset of volcanism in the Central Atlantic Magmatic Province and environmental change at the Triassic–Jurassic boundary, *Geology* 30 (2002) 267–270.
- [52] P.E. Olsen, D.V. Kent, H.-D. Sues, C. Koeberl, H. Huber, A. Montanari, E.C. Rainforth, S.J. Fowell, M.J. Szajana, B.W. Hartline, Ascent of dinosaurs linked to iridium anomaly at the Triassic–Jurassic boundary, *Science* 296 (2002) 1305–1307.
- [53] L.W. Alvarez, W. Alvarez, F. Asaro, H.V. Michel, Extraterrestrial sources for the Cretaceous–Tertiary extinction, *Science* 208 (1980) 1095–1108.
- [54] J. Pálffy, P.L. Smith, J.K. Mortensen, A U/Pb and  $^{40}\text{Ar}/^{39}\text{Ar}$  time scale for the Jurassic, *Can. J. Earth Sci.* 37 (2000) 923–944.
- [55] J. Pálffy, J.K. Mortensen, E.S. Carter, P.L. Smith, R.M. Friedman, H.W. Tipper, Timing the end-Triassic mass extinction: first on land, then in the sea? *Geology* 28 (2000) 39–42.
- [56] R. Mundil, I. Metcalfe, K.R. Ludwig, P.R. Renne, F. Oberli, R.S. Nicoll, Timing of the Permian–Triassic biotic crisis: implications from new zircon U/Pb age data (and their limitations), *Earth Planet. Sci. Lett.* 187 (2001) 131–145.
- [57] K. Min, R. Mundil, P.R. Renne, K.R. Ludwig, A test for systematic errors in  $^{40}\text{Ar}/^{39}\text{Ar}$  geochronology through comparison with U–Pb analysis of a 1.1 Ga rhyolite, *Geochim. Cosmochim. Acta* 64 (2000) 73–98.
- [58] K. Min, K.A. Farley, P.R. Renne, K. Marti, Single grain (U–Th)/He ages from phosphates in Acapulco meteorite and implications for thermal history, *Earth Planet. Sci. Lett.* 209 (2003) 323–337.